Passage of a vortex electron over an inclined grating

A. Pupasov-Maksimov [*]
Department of Mathematics, Universidade Federal de Juiz de Fora, Juiz de Fora, cep 36036-330, Brazil

D. Karlovets [†]
School of Physics and Engineering, ITMO University, 197101 St. Petersburg, Russia

(Received 19 December 2021; accepted 22 March 2022; published 11 April 2022)

We study Smith-Purcell radiation from a conducting grating generated by an inclined passage of a shaped electron wave packet with an electric quadrupole moment in the nonparaxial regime. Spreading of an asymmetric wave packet induces quadrupole corrections to the radiation field. Although the nonparaxial corrections stay small, they are dynamically enhanced during the interaction of the electron with the grating whose length exceeds the Rayleigh length of the packet. To simplify the possible experimental setup where such effects could be measured, we study the dependence of these effects on the inclination angle, i.e., the angle between the mean velocity of the packet and the surface of the grating. There is a minimal angle such that the multipole expansion always stays valid at the grating surface. In such a regime, the quadrupole contribution to the Smith-Purcell radiation can become the leading one, which represents a quantum effect impossible for classical pointlike electrons. Thus, the impact of the wave-packet shape (vortex structure or nonspherical shape) can be observed experimentally by comparing the radiation for different orientations of the grating in the single-electron regime.

DOI: 10.1103/PhysRevA.105.042206

I. INTRODUCTION

Many theoretical studies suggest that one can influence the properties of radiation or interactions of a free quantum particle with atoms and condensed matter by adjusting its wave-function shape [1–4]. As experimental capabilities increase, they enable studying vanishingly small interactions between quantum particles, condensed matter, and radiation, thus providing reliable experimental tools to test the fundamental theories [5–8].

In the present paper, we extend our previous studies [9,10]. of the Smith-Purcell radiation induced by shaped electron wave packets. A freely moving wave packet spreads. If such a packet carries a nonvanishing quadrupole momentum, then, according to the Heisenberg equations of motion, it has a quadratic dependence on the evolution time. The standard paraxial regime requires that the evolution time be small compared to the Rayleigh diffraction time.

We consider the nonparaxial regime of emission since the corresponding corrections become important already at moderate values of the orbital angular momentum (OAM) of vortex electrons [9,11]. A vortex electron carries an orbital angular momentum $\ell\hbar$ with respect to the propagation axis. Such a shaped wave packet is also characterized by multipole moments [12]. These multipole moments can be used to calculate the corrections dW_{eQ} and dW_{QQ} to the intensity dW_{ee} of Smith-Purcell radiation produced by a point charge when the quantum recoil η_q is small,

$$\eta_q := \frac{\omega}{\varepsilon} \ll \frac{dW_{eQ}}{dW_{ee}}, \quad \frac{\omega}{\varepsilon} \ll \frac{dW_{QQ}}{dW_{ee}}, \tag{1}$$

and the energy losses stay negligible compared to the electron's energy. We emphasize that there are two types of quantum corrections to the classical radiation of charge [13–17]: (1) the corrections due to recoil, which appear in the operator method [17] and the eikonal method [16], and (2) the corrections due to the finite coherence length of the emitting particle, which appear in the *nonparaxial* regime of emission [9].

The latter effects are usually neglected in the conventional paraxial regime, where the packets are almost plane waves. The nonparaxial regime, on the contrary, implies that one cannot neglect the spreading of the packet.

In the emission of photons by electrons, a comparison of the quantum calculations with the classical theory with the point electrons and a localized current implies the correspondence principle—the classical result should be recovered in a certain limiting case. Although it is often the case even when using the unlocalized plane-wave states of electrons [13], a thorough comparison with the classical theory implies the postselection of the emitting electrons in the same quantum state as they were in before emitting the photon. Depending on the electron states and on an experimental setup, this might be an additional experimental challenge. However, the photon emission measurements within the scheme with no postselection of the final electrons, which is the more frequently used one, cannot generally be compared with the classical theory at all, even if the recoil is small, because there is no classical

[*]tretiykon@yandex.ru
[†]d.karlovets@gmail.com

limit of this procedure. For this reason, below we adhere to the postselection scheme in which the final electron is also detected as a vortex state in coincidence with the photon. Such a scheme provides the most adequate test bed for comparison with the classical results with the point emitters, even though it might seem to be not the most experimentally convenient one. In this sense, the question of whether we follow the point-emitter interpretation or the one with the spatially extended charge [9,18] is secondary. We simply perform the quantum calculations as follows from the QED first principles with the final electron being postselected to the vortex state, as explained in Ref. [9], and then make a comparison with the classical predictions. A fully quantum study of the influence of the postselection procedure on a photon quantum state in a generic emission process is presented in Ref. [19].

Compared to the Cherenkov radiation or transition radiation from vortex electrons [4,20–22], the Smith-Purcell radiation is a better candidate to study the influence of the electron wave packet spreading on the radiation characteristics because the radiation formation length is defined by the grating length and, therefore, it can relatively easily be changed and compared to the Rayleigh length of the electron packet.

Our previous analytical results [9,10] highlight three observable effects related to the quadrupole moment and spreading of the wave packet. In contrast to a classical spreading beam, the spreading of the quantum wave packet does not lead to spectral line broadening. Numerical studies of the spectral lines reveal not only an absence of the broadening, but even *a slight narrowing* of the lines due to the charge-quadrupole interference. The quadrupole contribution is dynamically enhanced along the grating, leading to *a nonlinear growth* of the radiation intensity with the grating length. At the same time, the maximum of the radiation intensity with respect to the polar angle is shifted towards smaller angles. The magnetic dipole moment results in a small asymmetry of azimuthal distribution both for diffraction and Smith-Purcell radiation [4,9,10]. Nevertheless, the corresponding correction stays small for Smith-Purcell radiation, and we will not consider this contribution here.

For a direct experimental test, the radiation obtained in various experimental arrangements can be compared: with gratings of different lengths, or with different ratios of the initial mean radius $\bar{\rho}_0$ to the OAM of the packet, ℓ. However, the experimental task of *isolating small effects on radiation intensity from systematical effects* can be challenging. Instabilities in the wave-packet impact parameter, mean velocity β, various gratings' parameters, etc., could blur the nonparaxial effects. The usage of a single beam source and a single grating can simplify the possible experimental studies significantly.

Therefore, in the present paper we consider the case of an inclined passage of a wave packet to provide a theoretical prediction of the dependence of nonparaxial effects on the inclination angle. When the inclination angle φ_I is positive (see Fig. 1), motion away from the grating can extend the permitted passage time, and as a result, an increase of nonparaxial contributions can be expected. Let t_d be the diffraction time of the packet. Generally, when the inclination angle

$$\tan\varphi_I > \bar{\rho}_0/(\beta t_d),$$

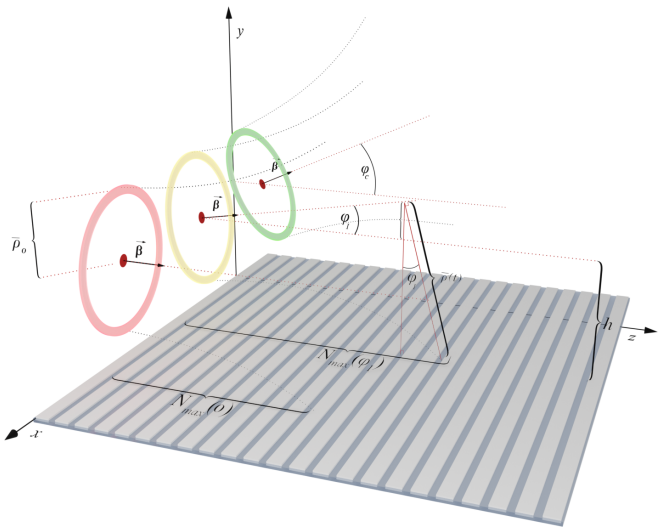

FIG. 1. Variation of the inclination angle, i.e., the angle between the mean velocity of the packet and the grating, results in the modification of the interaction length and effective impact parameter. Dashed lines indicate spreading of the wave packets. While the charge contribution (exponentially) decreases with the inclination angle, the quadrupole contribution is increased when $0 < \varphi_I < \varphi_c$.

the packet will always stay above the grating. Thus, one can formally consider an inclined passage over an infinite grating. Since the distance between the charge and the grating is increased in this case, the relative intensities of charge and quadrupole contributions can be changed by adjusting the inclination angle. This adjustment can be done simply by rotating the grating without changing the rest of the experimental setup, thus simplifying possible experimental studies.

Another potential application of our calculations is estimation of the beam spreading effects in the single-electron regime, i.e., a distribution of individual inclination angles and impact parameters of each wave packet. In this case, it is necessary to incoherently average the radiation intensities of the charge and quadrupole contributions over a reasonable distribution of impact parameters and inclination angles, which we expect to be a Gaussian distribution.

The paper is organized as follows. First, in Sec. II, we generalize our considerations for arbitrary axially symmetric wave packets with a quadrupole moment. The corresponding intrinsic quadrupole moment is characterized by the function $Q(t) = Q_0 + Q_2 t^2$, and the constants Q_0, Q_2 are related to the quadrupole contribution and the nonparaxial corrections. Within the multipole expansion, electromagnetic fields of an arbitrary axially symmetric wave packet can be calculated using expressions from Ref. [12]. This allows us to apply the method of generalized surface currents [23–25], with incident fields obtained by planar rotation (see Fig. 1) of the electromagnetic fields [11]. Calculations of the radiation fields in the wave zone in the Appendix, Sec. A 2 and the spectral and angular distribution of the radiation in Sec. III follow the line of Ref. [10]. The inclination angle results in the modification of the effective impact parameter and the appearance of an effective grating length. To study angular distributions, we apply numerical integration in the vicinity of the first spectral maximum.

The detailed physical model allows us to estimate the values of the following parameters, including the size of the wave packet and its aspect ratio, the orbital angular momentum, velocity, etc., that are compatible with our calculation scheme based on multipole expansion. Note that a single-electron regime with a freely propagating packet is realized for low electron currents, much lower than the so-called start current, which is usually less than 100 nA for the electron energy used in a transmission electron microscope (TEM) [26].

With obtained analytical expressions, in Sec. IV, we analyze how the quadrupole contribution can be isolated by changing the inclination angle. In the Conclusion, we discuss our final experimental proposal for the detection of the quadrupole (nonparaxial) contribution to the Smith-Purcell radiation. Our method is compatible both with moderate OAM values of $\ell \sim 10$ (see also Refs. [27–29]) and the large aspect ratio of Gaussian wave packets.

Throughout the paper, we use the units with $\hbar = c = |e| = 1$.

II. WAVE PACKETS WITH INTRINSIC MULTIPOLE MOMENTS

A. Gaussian packets and nonparaxial regime

It is shown in Ref. [9] that both the shape and the phase of the electron wave function can affect the transition amplitudes depending on how the final electron is detected. In classical electrodynamics, multipole moments describe electromagnetic fields generated by a discrete or continuous charge distribution. In particular, the quadrupole moment describes the deviation of the charge distribution from spherical symmetry.

In Refs. [9,10], the generalized Laguerre-Gaussian (LG) packet was used to describe a vortex electron with an electric quadrupole moment [11,30],

$$Q_{\alpha\beta}(t) = [\bar{\rho}(t)]^2\,\mathrm{diag}\{1/2,\,1/2,\,-1\}. \tag{2}$$

This quadrupole moment increases together with the mean radius of the wave packet,

$$\bar{\rho}(t) = \bar{\rho}_0\sqrt{1 + t^2/t_d^2}.$$

In this work, we generalize our previous results to arbitrary wave packets carrying an electric quadrupole moment. The simplest wave packet possessing a nonvanishing quadrupole moment is a Gaussian wave packet with different uncertainties

$$\sigma_x,\ \sigma_y,\ \sigma_z. \tag{3}$$

We isolate the intrinsic quadrupole moment, following Ref. [12]. Due to the spreading of this free wave packet, its quadrupole moment has a quadratic growth with time,

$$Q_{ii}(t) = 2\sigma_i^2 - \sigma_j^2 - \sigma_k^2 + t^2\frac{\lambda_c^2}{4}\left(\frac{2}{\sigma_i^2} - \frac{1}{\sigma_j^2} - \frac{1}{\sigma_k^2}\right),$$
$$(i,\,j,\,k) = \mathrm{cycle}(x,\,y,\,z), \quad Q_{xy}(t) = Q_{yz}(t) = Q_{xz}(t) = 0. \tag{4}$$

Note that in the spherically symmetric case, the quadrupole moment vanishes. The case of an axially symmetric Gaussian wave packet, $\sigma_x = \sigma_y = \sigma_\perp$, is analogous to the nonparaxial Laguerre-Gaussian wave packet, and the quadrupole moment tensor reads

$$Q_{\alpha\beta}(t) = Q(t)\mathrm{diag}\{1,\,1,\,-2\}, \tag{5}$$

$$Q(t) = \left(\sigma_\perp^2 - \sigma_z^2\right)\left(1 - \frac{\lambda_c^2 t^2}{4\sigma_\perp^2\sigma_z^2}\right) = Q_0 + Q_2 t^2. \tag{6}$$

Moreover, using the symmetry considerations and Heisenberg equations for the quadrupole moment, one can find that (5) and (6) are valid for arbitrary axially symmetric free wave packets. As a result, in this case, all the calculations of Smith-Purcell radiation can be made just by substituting $\bar{\rho}_0^2 \to Q_0$ and $\ell^2\frac{\lambda_c^2}{\bar{\rho}_0^2} \to Q_2$.

Note that an axially symmetric wave packet without OAM implies that $Q_0 Q_2 < 0$, while in the case of an LG packet, we have $Q_0 > 0$, $Q_2 > 0$. For the LG packet, there is a special case when the packet has the same diffraction time in all directions. This vortex packet spreads, and its transverse area is doubled during the diffraction time t_d,

$$t_d = \frac{m\bar{\rho}_0^2}{|\ell|} = \frac{t_c}{|\ell|}\left(\frac{\bar{\rho}_0}{\lambda_c}\right)^2 \gg t_c, \tag{7}$$

which is large compared to the Compton timescale $t_c = \lambda_c/c \approx 1.3\times10^{-21}$ s, $\lambda_c \approx 3.9\times10^{-11}$ cm. Moreover, the proportions between its transverse and longitudinal dimensions remain unchanged. The quadrupole moment (2) follows the same law (it is doubled during the diffraction time), and as a result, it increases monotonically.

For a Gaussian wave packet, such a uniform spreading requires spherical symmetry of the packet, thus leading to a vanishing quadrupole moment. In general, the packet will invert its aspect ratio during the spreading. As a result, $\mathrm{sgn}\,Q_0 \neq \mathrm{sgn}\,Q_2$, and the components of the quadrupole moment change their sign.

B. Geometrical restrictions

When the LG packet moves nearby the grating, its finite spreading time (7) puts an upper limit on the possible impact parameter h, on the initial mean radius of the packet, and on the grating length for a given inclination angle φ_I. The geometry (see Fig. 1) yields the following inequality,

$$\bar{\rho}(t)\cos\varphi_I < \beta t\sin\varphi_I + h, \tag{8}$$

which can be solved to find the maximum passage time,

$$t < t_{\max}(\phi_I)$$
$$= t_d\frac{\beta t_d h\sin\varphi_I + \bar{\rho}_0\cos\varphi_I\sqrt{h^2 + \bar{\rho}_0^2\cos^2\varphi_I + \beta^2 t_d^2\sin^2\varphi_I}}{\bar{\rho}_0^2\cos^2\varphi_I - \beta^2 t_d^2\sin^2\varphi_I}. \tag{9}$$

Note that the singularity of the denominator defines the critical angle

$$\tan\varphi_c = \frac{\bar{\rho}_0}{\beta t_d}, \tag{10}$$

and the passage time is unlimited for $\varphi_I > \varphi_c$. Therefore, in the following, the estimates on the maximum time and maximum grating length are considered only when $\varphi_I < \varphi_c$.

The maximum number of strips $N_{\max}(\varphi_I)$ is

$$N_{\max}(\varphi_I) = \beta t_{\max}/d,$$
$$N_{\max}(\varphi_I > \varphi_c) = \infty. \tag{11}$$

Note that in the experiment, the number of strips can be larger than $N_{\max}$, and when $N > N_{\max}$, the electrons may collide with the grating. However, the grating transition radiation, which is produced by electron collisions with the grating, should not affect the radiation pattern at larger polar angles. Therefore, we take $N_{\max}(\varphi_I)d$ as the formation length for the Smith-Purcell radiation when the inclination angles obey $\varphi_I < \varphi_c$.

The geometry implies that $\bar{\rho}_0 < h = \bar{\rho}(t_{\max})$, or $\bar{\rho}_0 \ll h$ for a long grating. In practice, only low diffraction orders can be considered, so that $d \sim \beta\lambda$ for the emission angles $\Theta \sim 90^\circ$. In the case of a parallel passage, a rough estimate of the maximum number of strips for $h \approx h_{\text{eff}} \sim 0.1\lambda$, $\beta \approx 0.5$, $\bar{\rho}_0 \sim 1$ nm yields [10]

$$N_{\max}(\varphi_I = 0) \lesssim \frac{h\bar{\rho}_0}{|\ell|\lambda\lambda_c} \sim \frac{10^3}{|\ell|}. \tag{12}$$

Hence, if $N_{\max}(\varphi_I = 0) \gg 1$, then $|\ell| < 10^3$.

C. Electric fields of the quadrupole moment

The physical mechanism of Smith-Purcell radiation is related to the polarization and surface currents induced by the electromagnetic interaction of a passing charge with the grating [23,25]. To calculate the surface current, we need only the electric fields. In the Cartesian coordinates x', y', z' aligned with the vector of the mean velocity of the wave packet, the electric field of the quadrupole moment can be calculated as follows [11],

$$\boldsymbol{E}_Q(\boldsymbol{r}', t) = \frac{\gamma}{4R'^3}\boldsymbol{\rho}'\left\{3\frac{Q_0}{R'^2}\left(1 - 5\frac{R_{z'}^2}{R'^2}\right) + Q_2\left[3\frac{T_{z'}^2}{R'^2}\left(1 - 5\frac{R_{z'}^2}{R'^2}\right) + 3\frac{R_{z'}^2}{R'^2} - 6\beta\frac{R_{z'}T_{z'}}{R'^2} - 1\right]\right\}$$
$$+ \frac{\gamma}{4R'^3}(\boldsymbol{z}' - \boldsymbol{\beta}t)\left\{3\frac{Q_0}{R'^2}\left(3 - 5\frac{R_{z'}^2}{R'^2}\right) + Q_2\left[\frac{T_{z'}^2}{R'^2}\left(3 - 5\frac{R_{z'}^2}{R'^2}\right) + 3\frac{R_{z'}^2}{R'^2} - 1\right]\right\}, \tag{13}$$

where the following notations are used: $\boldsymbol{\beta} = (0, 0, \beta)$, $\boldsymbol{z}' = (0, 0, z')$,

$$\boldsymbol{\rho}' = \{x', y'\}, \quad R_{z'} := \gamma(z' - \beta t), \quad T_{z'} := \gamma(t - \beta z'),$$
$$\boldsymbol{R}' = \{\boldsymbol{\rho}', \gamma(z' - \beta t)\}, \quad \gamma = (1 - \beta^2)^{-1/2}. \tag{14}$$

Note the complex time dependence of the quadrupole field in a fixed point of grating. First, the time dependence is included in the change of the distance between the packet and a fixed point. Second, there is an additional time dependence due to the terms proportional to $T_{z'}, T_{z'}^2$.

The transformation from the accompanying coordinate frame to the laboratory frame (see also Fig. 2) reads

$$x' = x,$$
$$y' = (y - h)\cos(\varphi_I) - z\sin(\varphi_I),$$
$$z' = z\cos(\varphi_I) + (y - h)\sin(\varphi_I). \tag{15}$$

The components of the electric field in the two coordinate systems are related by the rotation

$$E_x = E_{x'},$$
$$E_y = E_{y'}\cos(\varphi_I) + E_{z'}\sin(\varphi_I),$$
$$E_z = E_{z'}\cos(\varphi_I) - E_{y'}\sin(\varphi_I). \tag{16}$$

Following the generalized surface current model developed in Ref. [23], the radiation fields at large distances are written as

$$\boldsymbol{E}^R \approx \frac{i\omega e^{ikr_0}}{2\pi r_0}\int \boldsymbol{e}_0 \times [\boldsymbol{n} \times \boldsymbol{E}(k_x, y, z, \omega)]e^{-ik_z z}dz, \tag{17}$$

where the electric field $\boldsymbol{E} = \boldsymbol{E}_e + \boldsymbol{E}_Q$ is a sum of the Coulomb field of the charge and the electric field of the quadrupole moment. In the case of Smith-Purcell radiation, the integration is performed along the periodic grating. This expression is obtained for the far-field region, where the curl can be substituted by $\boldsymbol{e}_0$. The current density induced by the incident field,

$$\boldsymbol{j}(w) = \frac{1}{2\pi}\boldsymbol{e}_0 \times [\boldsymbol{n} \times \boldsymbol{E}(w)], \tag{18}$$

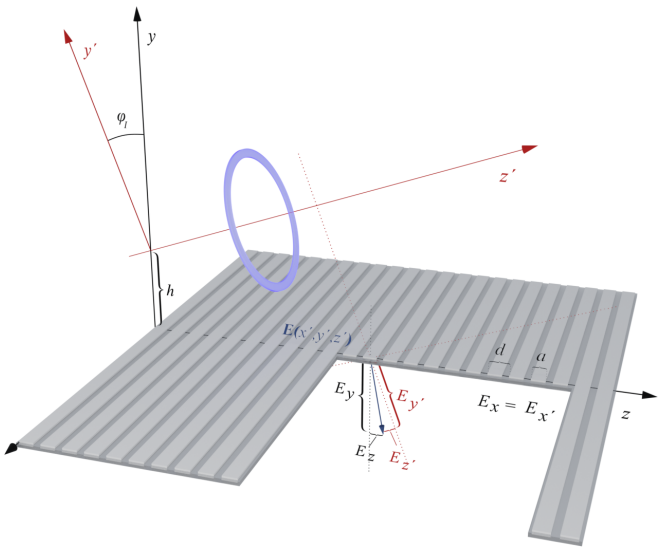

FIG. 2. Inclined passage of a Laguerre-Gaussian (LG) packet with respect to the conducting grating with the period d and width of the strip a. The electric fields of the packet induce surface currents on the grating, which are the source of the radiation. The transformation from the (x', y', z') to (x, y, z) coordinate system, and the transformation of the electric field components are given in (15) and (16).

is defined by a vector product of $\boldsymbol{E}$, i.e., the electromagnetic field of the electron incident on the surface of an ideally conducting grating, a normal to the surface $\boldsymbol{n}$, and the unit vector

$$\boldsymbol{e}_0 = \frac{\boldsymbol{r}_0}{|\boldsymbol{r}_0|} = (\sin\Theta\cos\Phi, \sin\Theta\sin\Phi, \cos\Theta).$$

For moderate electron energies required for the observation of the effects discussed in this work, the normal component of the surface current is crucial: For this reason, we employ the model of Ref. [23], which is more general than that of Brownell *et al.* [24].

D. Surface currents and radiation field

When the Fourier transform of xt is performed [see the Appendix, Sec. A 2 and Eq. (A9)], the surface current density

$$\boldsymbol{j} = \frac{1}{2\pi}(-E_x e_{0y}, E_x e_{0x} + E_z e_{0z}, -E_z e_{0y})$$

reads

$$\boldsymbol{j}(k_x, y', z', \omega) = \exp\left(iz'\frac{\omega}{\beta}\right)[\boldsymbol{j}_0(k_x, y', \omega) + \boldsymbol{j}_{Q_1}(k_x, y', \omega)z' + \boldsymbol{j}_{Q_2}(k_x, y, \omega)z'^2], \quad (19)$$

where y' and z' should be substituted via (15). The first term contains generalized currents, which are uniform along the grating, $\boldsymbol{j}_0(k_x, y', \omega) = \boldsymbol{j}_e(k_x, y', \omega) + \boldsymbol{j}_{Q_0}(k_x, y', \omega)$, while the next terms are related to the linear and quadratic time-dependent quadrupole contributions.

The integration with respect to the z coordinate along the periodic grating

$$\int_0^{Nd} dz(\boldsymbol{j}_0 + \boldsymbol{j}_{Q_1} z + \boldsymbol{j}_{Q_2} z^2)\exp\{iz[\omega\Theta_I + i\sin(\varphi_I)\mu]\} = \left[\boldsymbol{j}_0 + \boldsymbol{j}_{Q_1}(-i\partial_{\Omega_I}) + \boldsymbol{j}_{Q_2}(-i\partial_{\Omega_I})^2\right]F_I(\Omega_I), \quad (20)$$

can be performed using the derivatives of the following *generating function*,

$$F_I(\Omega_I) = \sum_{j=0}^{N}\int_{jd}^{jd+a} dz\exp\{iz[\Omega_I + i\sin(\varphi_I)\mu]\} = \frac{2\sin\left(\frac{a(\Omega_I+iM_I)}{2}\right)}{(\Omega_I + iM_I)}\frac{\sin\left(\frac{Nd(\Omega_I+iM_I)}{2}\right)}{\sin\left(\frac{d(\Omega_I+iM_I)}{2}\right)} \times \exp\left(\frac{(i\Omega_I - M_I)}{2}[a + (N-1)d]\right), \quad (21)$$

with respect to the parameter Ω_I, where

$$\Theta_I = \frac{\cos(\varphi_I)}{\beta} - \cos(\Theta), \quad \Omega_I = \omega\Theta_I,$$
$$M_I = \sin(\varphi_I)\mu = \sin(\varphi_I)\sqrt{\frac{\omega^2}{\gamma^2\beta^2} + k_x^2}. \quad (22)$$

Due to the inclined path of the wave packet, the singularity of the denominator in (21) shifts to the complex frequency

$$\omega = \left(\frac{2\pi g}{d} + i\sin(\varphi_I)\sqrt{\frac{1}{\gamma^2\beta^2} + \sin^2\Theta\cos^2\Phi}\right) \times \left(\frac{\cos(\varphi_I)}{\beta} - \cos(\Theta)\right)^{-1}. \quad (23)$$

Its real part corresponds to the resonance peaks

$$\omega_g = \frac{2\pi}{\lambda_g} = \frac{2\pi g}{d}\left(\frac{\cos(\varphi_I)}{\beta} - \cos(\Theta)\right)^{-1}, \quad g = 1, 2, 3, \ldots, \quad (24)$$

which is slightly shifted compared to the case of the parallel passage. We can estimate the width of the spectral lines as follows. When the passage is parallel, the width

$$\Gamma = \frac{\delta\omega}{\omega} = \frac{1}{N} \quad (25)$$

is related to the finite grating length. In other words, the integration of $\exp(iz\omega)$ is performed over a finite interval. Alternatively, one can integrate over the whole semi-infinite line introducing a small imaginary shift $\exp[iz(\omega + i\Gamma)]$. Since the inclination results in such a small imaginary shift, we obtain the spectral width

$$\Gamma_I = \frac{1}{N} + \sin(\varphi_I)\sqrt{\frac{1}{\gamma^2\beta^2} + \cos^2\Phi\sin^2\Theta}. \quad (26)$$

Hereinafter, the effective number of strips is equal to

$$N_{\text{eff}} = \frac{1}{\Gamma_I} = \frac{N}{1 + N\sin\varphi_I\sqrt{\frac{1}{\gamma^2\beta^2} + \cos^2\Phi\sin^2\Theta}}. \quad (27)$$

When the inclination angle is positive, the grating can be considered as infinite, and the corresponding limit is written as

$$F_{I,\infty}(\Theta_I) = \lim_{N\to\infty} F_I(\Theta_I) = \frac{1}{(M_I - i\Omega_I)}\frac{\exp[(i\Omega_I - M_I)a] - 1}{\exp[(i\Omega_I - M_I)d] - 1}. \quad (28)$$

In the following text, these compact notations are used:

$$\partial_{\Omega_I}F_I(\Omega_I) = F_I'(\Omega_I), \quad \partial^j_{\Omega_I}F_I(\Omega_I) = F^{(j)}(\Omega_I).$$

III. MULTIPOLE CORRECTIONS TO THE SMITH-PURCELL RADIATION FROM THE LG WAVE PACKET

A. Spectral distribution of the Smith-Purcell radiation from the LG wave packet

The distribution of the radiated energy over the frequencies and angles,

$$\frac{d^2W}{d\omega d\Omega} = r_0^2|\boldsymbol{E}^R|, \quad (29)$$

is a sum of the following terms:

$$dW_{ee} = \frac{\omega^2}{4\pi^2}|\boldsymbol{j}_e|^2|F_I(\Omega_I)|^2, \tag{30}$$

$$dW_{eQ_k} = i^k\frac{\omega^2}{4\pi^2}\left[\boldsymbol{j}_e\boldsymbol{j}^*_{Q_k}F_I(\Omega_I)F_I^{(k)}(\Omega_1)^* + (-1)^k\boldsymbol{j}^*_e\boldsymbol{j}_{Q_k}F_I(\Omega_1)^*F_I^{(k)}(\Omega_1)\right], \tag{31}$$

$$dW_{Q_jQ_k} = \frac{(-i)^{j+k}\omega^2}{4\pi^2}\left[(-1)^k\boldsymbol{j}_{Q_j}\boldsymbol{j}^*_{Q_k}F_I^{(j)}(\Omega_I)F_I^{(k)}(\Omega_I)^* + (-1)^j\boldsymbol{j}^*_{Q_j}\boldsymbol{j}_{Q_k}F_I^{(j)}(\Omega_I)^*F^{(k)}(\Omega_I)\right]. \tag{32}$$

Then, the radiation of a charge with inclined passage over an infinite grating is

$$\begin{aligned}\frac{d^2W_{e,I\infty}}{d\omega d\Omega} = {}& \exp\left(-\frac{\omega h_I}{\beta\gamma}\sqrt{1+\beta^2\gamma^2\cos^2\Phi\sin^2\Theta}\right)\frac{\left\{\cos(a\omega\Theta_I) - \cosh\left[a\omega\sin(\varphi_I)\sqrt{1/(\beta^2\gamma^2)+\cos^2\Phi\sin^2\Theta}\right]\right\}}{\left\{\cos(d\omega\Theta_I) - \cosh\left[d\omega\sin(\varphi_I)\sqrt{1/(\beta^2\gamma^2)+\cos^2\Phi\sin^2\Theta}\right]\right\}}\\
&\times (1+\beta^2\gamma^2\cos^2\Phi\sin^2\Theta)^{-1}\{[\cos^2(\Theta)+\sin^2(\Phi)\sin^2(\Theta)][\cos^2(\varphi_I)+\gamma^2\sin^2(\varphi_I)] + \beta\gamma^2\cos^2(\Phi)\sin^2(\Theta)\\
&\times [2\cos(\varphi_I)\cos(\Theta) + \beta\gamma^2\cos^2(\Theta)\sin^2(\varphi_I) + \beta\gamma^2\sin^2(\Theta)[1+\sin^2(\Phi)\sin^2(\varphi_I)]]\}\\
&\times [\gamma^2\cos^2(\varphi_I) - 2\beta\gamma^2\cos(\varphi_I)\cos(\Theta) + \beta^2\gamma^2\cos^2(\Theta) + \sin^2(\varphi_I)(1+\beta^2\gamma^2\cos^2\Phi\sin^2\Theta)]^{-1}.\end{aligned} \tag{33}$$

Because of the inclination, the impact parameter is included in the exponential factor in combination with the strip length a and period d,

$$h_I = 2h\cos(\varphi_I) + (a-d)\sin(\varphi_I). \tag{34}$$

One can see that the angular dependence of $d^2W_{e,I\infty}$ becomes d^2W_e when the inclination angle is zero. When $a = d$, our result coincides with the case of radiation diffraction on a conducting semiplane [31].

The quadrupole contributions from $\boldsymbol{j}_{Q_1}$ and $\boldsymbol{j}_{Q_2}$ are defined by the real parts of the product of currents, and by the form factor F_I and its derivatives. Nevertheless, explicit calculations show [32] that these terms also have a factorized structure,

$$\begin{aligned}dW_{eQ_j} = {}& \exp\left(-\frac{\omega h_I}{\beta\gamma}\sqrt{1+\beta^2\gamma^2\cos^2\Phi\sin^2\Theta}\right)\\
&\times P_{eQ_j}(k_x, y, \omega)F_{eQ_j}(\omega, k_z).\end{aligned} \tag{35}$$

Here, the functions $P_{eQ_j}(k_x, y, \omega)$ define the angular distributions, and $F_{eQ_j}(\omega, k_z)$ determine the positions of the spectral lines and their width [therefore, we will call $F_{eQ_j}(\omega, k_z)$ *a spectral factor*]. In Fig. 3, we compare the intensities of radiation from the charge, the quadrupole, and from their interference. It can be seen that the radiation from the wave packet decreases more slowly compared to the charge radiation (or a wave packet with no quadrupole moment) when the inclination is increased. The spectral line of the wave-packet radiation is also slightly sharper.

For parallel passage, the charge and the charge-quadrupole contributions have almost the same azimuthal dependence (42), which is defined mostly by the exponential factor for $\beta \sim 0.5$. In the case of an inclined passage, these azimuthal dependencies should be (linearly) mixed after the linear transformation of the fields and the coordinate transformations. However, since they all have the same form (for those parameters that we have already investigated), this mixing will have little effect on the azimuthal distributions.

B. Qualitative analysis and multipole expansion

We suppose that the axially symmetric wave packet is shaped to have only a nonvanishing electric quadrupole moment, similar to the case of (2) (a vortex wave packet) or (5) (Gaussian wave packet). In this case, the total radiation intensity dW includes classical radiation from the point charge dW_{ee}, the interference term dW_{eQ}, and the radiation from quadrupole dW_{QQ}:

$$\frac{dW}{d\omega d\Omega} \equiv dW = dW_{ee} + dW_{eQ} + dW_{QQ}. \tag{36}$$

In the case of a Gaussian wave packet, higher-order multipole moments vanish. For Laguerre-Gaussian packets, higher-order multipole moments are small compared to the dipole and quadrupole ones, and this formula can be considered an approximation. This perturbative regime was derived from QED

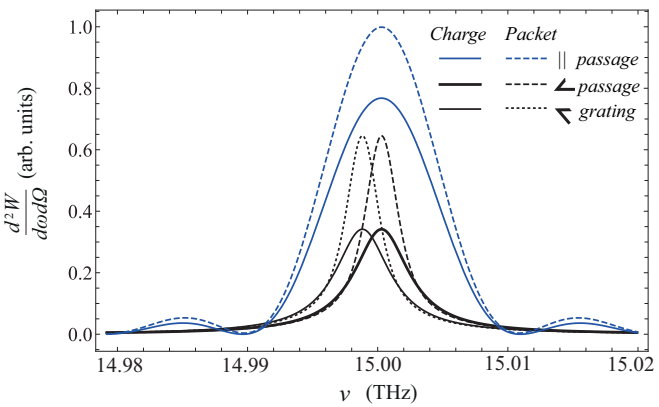

FIG. 3. Comparison of the radiation spectrum of a classical point emitter (solid curves) and of a vortex electron packet (dashed curves) for the parallel passage and the inclined passage with a critical inclination $\varphi_I = 0.0045^\circ$ defined by the impact parameter $h = 2.8\ \mu$m, $\bar{\rho}_0 = 100$ nm, $\ell = 10$, $\beta = 0.5$. The effects of beam and grating inclinations are compared. A zenith direction perpendicular to the grating plane $\Theta = \Phi = \frac{\pi}{2}$ is considered. The grating period $d = 0.01$ mm, $a = d/2$, and the number of strips $N = 3500$.

in the quasiclassical approximation when the final electron is detected in the vortex state [9].

For parallel passage, we neglected the dW_{QQ} contribution because of the finite grating length. In the case of infinite grating, an inclined passage with a valid multipole expansion is possible, therefore, we should keep this term. In the case of inclined passage, all considerations of Ref. [10] are still valid. We only need to substitute $N_{\max}$ by N_{eff} from (27). For a large $N_{\max}$ or for inclination angles larger than the critical one, $\varphi_I > \varphi_c$, when $N_{\max} = \infty$, we can estimate $N_{\text{eff}} = \beta\gamma/\sin(\varphi_I)$.

Using the explicit formulas (31) (see also Ref. [10]), one can distinguish three different corrections from the charge-quadrupole interference: dW_{eQ_0}, dW_{eQ_1}, and dW_{eQ_2}. Their relative contributions are

$$\frac{dW_{eQ_0}}{dW_{ee}} \sim \eta_{Q_0} := \frac{\bar{\rho}_0^2}{h_{\text{eff}}^2}$$

quasiclassical quadrupole contribution, (37)

$$\frac{dW_{eQ_1}}{dW_{ee}} \sim \eta_{Q_1} := \ell^2 \frac{\lambda_c^2}{\bar{\rho}_0^2}$$

ordinary nonparaxial contribution [31], (38)

$$\frac{dW_{eQ_2}}{dW_{ee}} \sim \eta_{Q_2} := N_{\text{eff}}^2 \ell^2 \frac{\lambda_c^2}{\bar{\rho}_0^2}$$

dynamically enhanced nonparaxial contribution [11], (39)

where the effective impact parameter of Smith-Purcell radiation naturally appears

$$h_{\text{eff}} = \frac{\beta\gamma\lambda}{2\pi} = \frac{\beta\gamma}{\omega} \sim 0.1\lambda \quad \text{for } \beta \approx 0.4\text{–}0.8. \tag{40}$$

It follows from (39) that a large effective number of strips $N_{\text{eff}} \gg 1$ can lead to *the nonparaxial regime of emission* with

$$\eta_{Q_1} \ll 1, \quad \eta_{Q_2} \lesssim 1, \tag{41}$$

when the quadrupole contribution becomes noticeable.

All the inequalities and restrictions from Ref. [10] can be summarized as follows. *The packet radius should be smaller than the wavelength of the emitted radiation*. This is just a condition of the multipole expansion in the wave zone. In this case, we can also safely neglect the possible effects of wave-packet reduction due to the measurement of the electron position by observing an emitted photon.

Using the definition for the quantum and classical regimes by Renieri [33], such a wave packet should be considered within the "classical regime": *The electron operates in the finite-length homogeneously broadened classical regime if throughout the entire interaction length L its axial position can be quantum mechanically localized with an accuracy better than the wavelength of the electromagnetic force wave with which it interacts* [34]. However, despite the fact that the electron is well localized, the internal structure of the wave packet can be seen in the radiation intensity (see Ref. [9], Figs. 3 and 4). Modifications of the radiation intensity are created by the quadrupole moment, which is an entirely quantum characteristic of the wave packet. Therefore, we call this modification a nonlinear quantum effect.

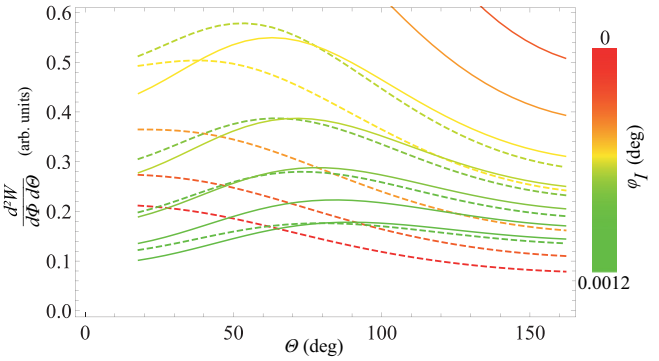

(a) $\ell = 10$, $h = 0.92\,\mu$m

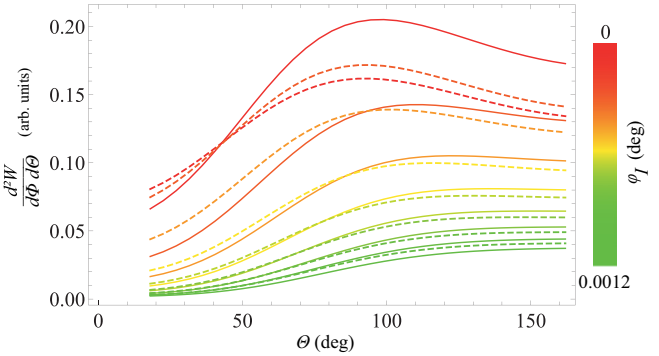

(b) $\ell = 10$, $h = 2.76\,\mu$m

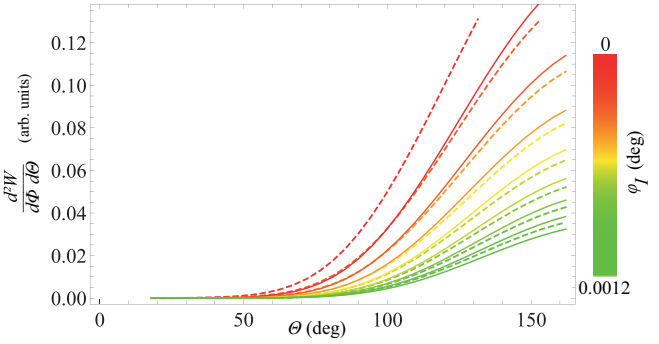

(c) $\ell = 10$, $h = 9.2\,\mu$m

FIG. 4. Polar dependence of radiation intensity in the case of a charge (solid lines) and a wave packet (dashed lines) when the inclination angle varies form 0 to $1.5\varphi_c$ (illustrated with a change of color from red to green—see the color bar). The number of strips $N_{\max}(\varphi_I = 0) = 1800$ for the parallel passage of the wave packet corresponds to the impact parameter $h = 2.8$ μm, velocity $\beta = 0.5$, period $d = 0.01$ mm, OAM $\ell = 10$, initial mean radius $\bar{\rho}_0 = 50$ nm, and grating length 2.5 cm.

In the case of an efficiently infinite grating, the energy losses of the electron may become noticeable, or its size can become larger than the wavelength emitted during its effective path $N_{\text{eff}}d$ over the grating. From the width of the spectral line we estimate

$$N_{\text{eff}} = \frac{\gamma\beta}{\sin\varphi_c} = \frac{\gamma\beta^2 t_d}{\bar{\rho}_0}.$$

Then, during the effective interaction time, the vortex wave packet will spread to

$$\bar{\rho}\left(\frac{N_{\text{eff}}d}{\beta}\right) = \bar{\rho}_0\sqrt{1+\gamma^2\beta^2\frac{d^2}{\bar{\rho}_0^2}}.$$

The resulting size should be small compared to the emitted wavelength,

$$\bar{\rho}_0^2 < \lambda^2 - \gamma^2\beta^2 d^2.$$

This condition is definitely violated when the right-hand side of the inequality is negative. This occurs when $\beta \geqslant 0.58$ (forward radiation) and $\beta \geqslant 0.78$ (vertical radiation). However, in this case N_{eff} is large, and very long gratings are required to fulfill this condition.

The baseline parameter set for the IR and THz radiation for parallel passage [10] is as follows: $\bar{\rho}_0 = 10^0$–10^2 nm, $\ell \sim 10^1$–10^3, $N \lesssim 10^0$–10^3.

IV. RADIATION INTENSITY FROM A WAVE PACKET AND A POINT CHARGE AS A FUNCTION OF THE INCLINATION ANGLE

To compare the radiation intensity from the wave packet and the point charge in a fixed direction, we need to integrate dW with respect to the frequency. At a nonzero inclination angle, the analytical integration of quadrupole terms seems to be impossible. However, numerical integration converges rapidly and allows visualization of the resulting angular distributions. We also test our numerical integration in the case of parallel passage, comparing it with the analytical angular distributions of the charge radiation in the main diffraction order $g = 1$,

$$\frac{dW_{ee}}{d\Omega} = N\frac{d^2\omega_1^3}{\pi^2}\sin^2\left(\frac{a\pi}{d}\right)\exp\left(-\frac{2\omega_1 y}{\beta\gamma}\sqrt{1+\beta^2\gamma^2\cos^2\Phi\sin^2\Theta}\right) \times \frac{\cos^2\Theta + 2\beta\gamma^2\cos^2\Phi\cos\Theta\sin^2\Theta + \sin^2\Phi\sin^2\Theta + \beta^2\gamma^4\cos^2\Phi\sin^4\Theta}{\beta^2\gamma^2(1+\beta^2\gamma^2\cos^2\Phi\sin^2\Theta)}, \tag{42}$$

which is valid for large N.

Since the polar distribution strongly depends on the impact parameter, in Fig. 4 we compared the evolution of polar distributions for varying inclination angles for different impact parameters. There is a competition between the dynamical enhancement of the quadrupole contribution and the general exponential decay of radiation intensity that occurs with increasing impact parameter or inclination angle. It can be seen that the polar distribution for wave packets is shifted to the smaller polar angles compared to the polar distribution of charge radiation, and it behaves differently under variations of the inclination angle. This confirms our idea that *one can distinguish radiation patterns from a wave packet and a point charge* by varying the inclination angles. The polar dependence of the radiation intensity may be a suitable candidate for experimental measurements. First, at the critical inclination angle, the change in the polar dependence is not small (see Fig. 4).

In Fig. 5 we fix a detector in the zenith direction $\Phi = \Theta = \pi/2$ and observe how the radiation intensity changes with variations of inclination angle. Radiation from the charge demonstrates exponential decay with increasing inclination angle. In contrast, for the wave packet, an initial increase of the inclination angle will lead to higher radiation intensities when the impact parameter does not exceed $2h_{\text{eff}}$. To explicitly show an interplay between the effective grating length which depends on the inclination and quadupole contribution we also calculate radiation intensities of a spherically symmetric Gaussian (SSG) wave packet. They are shown by the dotted lines in Fig. 5. We choose a spherically symmetric Gaussian wave packet with the same Rayleigh length as the LG packet, thus the corresponding effectige grating length is equal for both packets. In this case the difference with the radiation from the point charge is only due to effective grating length variations (the angle at which the dotted line coincides with the solid line corresponds to the minimal angle at a given impact parameter, when both packets pass above the grating). Thus, the difference between dotted and dashed lines is due to the quadrupole momentum contribution only.

The critical angle for $\ell = 10$ is rather small, $\varphi_c = 0.0089^\circ$, however, it is already within the currently available angular positioning technologies [35] with angular accuracy about 2 arcsec. The critical angle also can be scaled by a transition to a large OAM. In the case of $\ell = 100$, $\varphi_c = 0.089^\circ$, we can expect a strong manifestation of the quadrupole contribution, observing flat behavior of the radiation intensity for the inclination angles from 0 to 0.06°.

V. CONCLUSIONS

We have calculated Smith-Purcell radiation generated by a free-electron wave packet with an electric quadrupole moment in the range from THz to optical frequencies. Diffraction grating is assumed to be ideally conducting, and arbitrary inclination angles of the wave-packet passage are considered. The state of an electron can be described by the Gaussian-Laguerre wave packet with an orbital angular momentum or a Gaussian wave packet with an axial symmetry only. In the former case, the nonparaxial parameter is scaled with the OAM, while in the latter case, it depends on the aspect ratio of the wave packet. In the case of a Gaussian wave packet, our results are exact within the quasiclassical approximation.

As the electron moves near the grating, the spreading of the packet leads to an increase of the quadrupole moment, which also can be seen in the radiation. Although the quadrupole radiation is low as long as the multipole expansion stays valid (in practice, almost always), it leads to an interesting effect: While the radiation intensity from a charge linearly

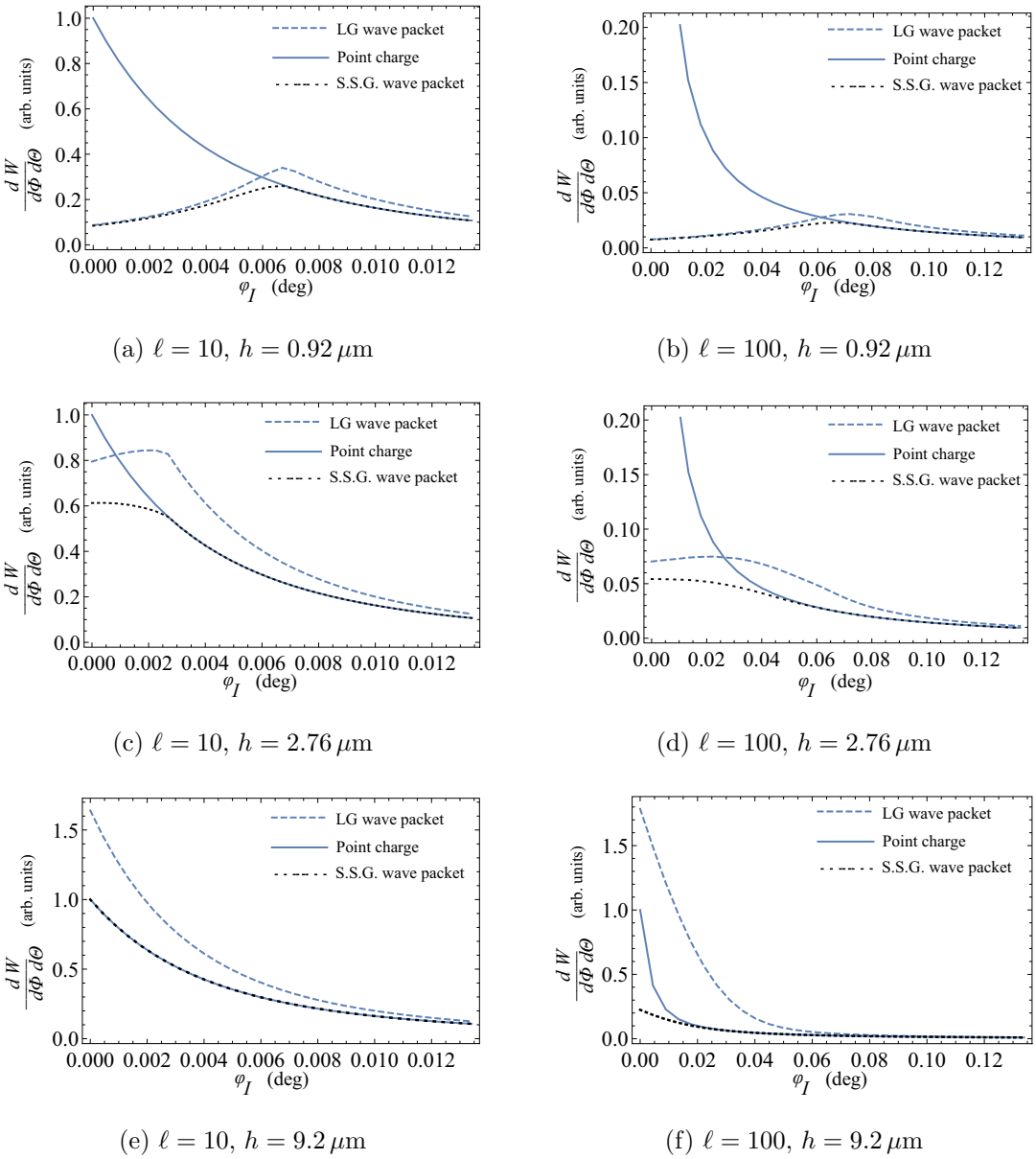

(a) $\ell = 10$, $h = 0.92\,\mu$m (b) $\ell = 100$, $h = 0.92\,\mu$m

(c) $\ell = 10$, $h = 2.76\,\mu$m (d) $\ell = 100$, $h = 2.76\,\mu$m

(e) $\ell = 10$, $h = 9.2\,\mu$m (f) $\ell = 100$, $h = 9.2\,\mu$m

FIG. 5. Radiation intensity in the vertical direction $\Theta = \Phi = \frac{\pi}{2}$ as a function of the inclination angle φ_I for an LG wave packet with OAM, compared to the radiation intensity from a point charge and a spherically symmetric Gaussian (SSG) wave packet. The effective impact parameter is $h_{\text{eff}} = 1.84\ \mu$m, number of strips $N = 2500$, velocity $\beta = 0.5$, period $d = 0.01$ mm, and the initial mean radius $\bar{\rho}_0 = 50$ nm.

increases with the number of the grating periods, the quadrupole contribution leads to a faster qubic growth, which resembles the coherence effect (superradiance) from a classical many-particle beam. However, in our problem, *this is a purely quantum effect of the spatial coherence of a vortex packet*. For relativistic particles, spreading can be neglected, but for nonrelativistic and even moderately relativistic electrons (with kinetic energies of 100–300 keV), this effect can lead to both a change in the angular distribution and an increase in the total radiation loss.

Note that a large OAM leads to a quick spreading and requires short gratings, while small OAM results in a relatively slow spreading and allows using longer gratings. Nevertheless, in the case of inclined passage, we can assume that the wave packets have a large OAM and small Rayleigh lengths.

We have shown a possibility to track the effects of the spatial coherence of the wave packets with intrinsic angular momentum by measuring the intensity of radiation with varying inclination angle (Fig. 5). The observed dependencies of the radiation intensity reveal a qualitative difference between the cases of a charge and a structured wave packet. The radiation of a charge demonstrates an exponential decrease with the inclination angle. In contrast, the radiation from a wave packet increases when $\varphi_I \in (0, 0.5\varphi_c)$ and the impact parameter $h < 2h_{\text{eff}}$. The critical angle is defined by the Rayleigh length, and in the case of a vortex electron, it is proportional to the OAM. Our calculations show that experimental observations of the quadrupole contribution to the Smith-Purcell radiation can be done with a moderate value of OAM, $\ell \sim 100$, or with Gaussian packets with large asymmetry. The reverse is

also true: An inverse problem can be used to determine the wave-packet "shape" by observing the resulting Smith-Purcell radiation, which provides a noninvasive experimental tool to study, for instance, vortex electrons.

ACKNOWLEDGMENTS

We are grateful to A. A. Tishchenko and P. O. Kazinski for fruitful discussions. We thank Lydia Pogorelskaya for careful reading of the manuscript and Ivan Pustovit for help with illustrations. The study in Sec. II is supported by the Russian Science Foundation (Project No. 17-72-20013). The studies of Sec. III are supported by the Ministry of Science and Higher Education of the Russian Federation (Agreement No. 075-15-2021-1349). The studies in Sec. IV are supported by the Government of the Russian Federation through the ITMO Fellowship and Professorship Program.

APPENDIX

1. Electromagnetic fields of LG wave packet in the rest frame

Consider a vortex electron described by the LG packet with $n = 0$ or an axially symmetric Gaussian wave packet with a nonunity aspect ratio. Its electromagnetic fields are a sum of those of the charge e and of the electric quadrupole moment $Q_{\alpha\beta}$, Eq. (5) (and of the magnetic moment $\boldsymbol{\mu}$ in the case of vortex electrons). The fields in cylindrical coordinates in the rest frame were calculated in Ref. [11]. In our problem, we prefer to use the Cartesian coordinates

$$
\begin{aligned}
E_x &= \frac{x}{r^3}\left(1+\frac{1}{4}\left\{\frac{3Q_0}{r^2}\left(1-5\frac{z^2}{r^2}\right)+Q_2\left[\frac{3t^2}{r^2}\left(1-5\frac{z^2}{r^2}\right)+3\frac{z^2}{r^2}-1\right]\right\}\right),\\
E_y &= \frac{y}{r^3}\left(1+\frac{1}{4}\left\{\frac{3Q_0}{r^2}\left(1-5\frac{z^2}{r^2}\right)+Q_2\left[\frac{3t^2}{r^2}\left(1-5\frac{z^2}{r^2}\right)+3\frac{z^2}{r^2}-1\right]\right\}\right),\\
E_z &= \frac{z}{r^3}\left(1+\frac{1}{4}\left\{\frac{3Q_0}{r^2}\left(3-5\frac{z^2}{r^2}\right)+Q_2\left[\frac{3t^2}{r^2}\left(3-5\frac{z^2}{r^2}\right)+3\frac{z^2}{r^2}-1\right]\right\}\right),\\
H_x &= \frac{z}{r^5}\left(3x\frac{l}{2m}-\frac{3}{2}Q_2 ty\right),\\
H_y &= \frac{z}{r^5}\left(3y\frac{l}{2m}-\frac{3}{2}Q_2 tx\right),\\
H_z &= \frac{l}{2m}\left(3\frac{z^2}{r^2}-1\right)\frac{1}{r^3},
\end{aligned}
\tag{A1}
$$

where in the case of an LG wave packet, we can just substitute $Q_0 = \bar{\rho}_0^2$, $Q_2 = \frac{l^2\lambda_c^2}{\bar{\rho}_0^2}$, and in the case of a Gaussian packet, we take $\ell = 0$ and

$$
Q_0 = \left(\sigma_\perp^2 - \sigma_z^2\right),
$$

$$
Q_2 = \left(\sigma_\perp^2 - \sigma_z^2\right)\frac{\lambda_c^2}{4\sigma_\perp^2\sigma_z^2}.
$$

We now transform these fields to the laboratory frame, where the particle moves along the z axis with a velocity $\langle u\rangle \equiv \beta$ according to the law

$$
\langle z\rangle = \beta t.
$$

Applying the Lorentz transformations, we obtain electric fields in the laboratory frame,

$$
\begin{aligned}
E_x^{(\mathrm{lab})} &= \gamma(E_x + \beta H_y),\\
E_y^{(\mathrm{lab})} &= \gamma(E_y - \beta H_x), \quad E_z^{(\mathrm{lab})} = E_z.
\end{aligned}
\tag{A2}
$$

Simultaneously, we need to transform the coordinates and the time as follows [36]:

$$
\begin{aligned}
&\boldsymbol{\rho} = \{x, y\} = \mathrm{inv}, \quad z \to \gamma(z-\beta t) =: R_z, \quad t \to \gamma(t-\beta z) =: T_z,\\
&r^2 \to [\rho^2 + \gamma^2(z-\beta t)^2], \quad \gamma = (1-\beta^2)^{-1/2}.
\end{aligned}
\tag{A3}
$$

We omit the magnetic fields, because to calculate the surface current in the following, we need only the electric field.

2. Fourier transform of the fields

First, we calculate the Fourier transform of the electric fields produced by the wave packet

$$\boldsymbol{E}(q_x, y', z', \omega) = \int dxdt\, \boldsymbol{E}(\boldsymbol{r}', t) e^{i\omega t - iq_x x}$$

in the coordinate system (x', y', z'). Note that $x' = x$. Thus, we obtain the same integrals as in Ref. [10]. Consider the general structure of these integrals,

$$\boldsymbol{E}(q_x, y', z', \omega) = \int dxdt\, \boldsymbol{f}(x, y', z') \frac{R_{z'}^n}{R'^{\frac{\nu}{2}}} e^{i\omega t - iq_x x} = \gamma^n e^{i\omega z'/\beta} f(i\partial_{q_x}, y', z')(i\beta\partial_\omega)^n e^{-i\omega z'/\beta} I_\nu(q_x, y', z', \omega), \tag{A4}$$

where $R_{z'} = \gamma(z' - \beta t)$ and $\boldsymbol{f}(x, y', z')$ are polynomial functions depending on x, y' variables (the maximum degrees of x, y' are equal to 1, and the maximum z' degree is 2 for the quadrupole contribution). Note that the master integrals

$$I_{2n+1}(q_x, y', z', \omega) = \int_{-\infty}^{\infty} dt \int_{-\infty}^{\infty} dx \frac{e^{i(\omega t - q_x x)}}{[x^2 + y'^2 + \gamma^2(z' - \beta t)^2]^{(2n+1)/2}} = \frac{2\pi}{\gamma\beta} \frac{i^{n+1}\mu^n h_{n-1}^{(1)}(i\mu|y'|)}{(2n-1)!!|y'|^{n-1}} \exp\left(\frac{iwz'}{\beta}\right), \quad n = 1, 2, 3. \tag{A5}$$

where $\mu = \sqrt{\frac{\omega^2}{\gamma^2\beta^2} + q_x^2}$, and $h_{n-1}^{(1)}$ are spherical Hankel functions of the first kind [37], which contain y' in the denominator. Nevertheless, the final expressions for the Fourier-transformed fields are polynomials in y', z', and $\mathrm{sgn}(y')$ (up to an exponential factor). It follows from the fact that the only singularity of fields $1/R$ has spherical symmetry. Such a structure is preserved after the coordinate substitution (15).

In particular, the electric field from the charge

$$\boldsymbol{E}_e(q_x, y', z', \omega) = \gamma[i\partial_{q_x}, y, (z' + i\beta\partial_\omega)] I_3(q_x, y', z', \omega), \tag{A6}$$

after the differentiation, reads

$$\boldsymbol{E}_e(q_x, y', z', \omega) = \frac{2\pi}{\beta}\left[-iq_x, \mathrm{sgn}(y')\sqrt{\left(\frac{\omega}{\beta\gamma}\right)^2 + q_x^2}, -i\frac{\omega}{\beta\gamma^2}\right] \frac{\exp\left\{iz'\frac{\omega}{\beta} - |y'|\sqrt{\left(\frac{\omega}{\beta\gamma}\right)^2 + q_x^2}\right\}}{\sqrt{\left(\frac{\omega}{\beta\gamma}\right)^2 + q_x^2}}. \tag{A7}$$

Calculations of (A4) for the quadrupole fields can be done with the aid of computer algebra (see the public repository [38]). In the case of the inclined passage, we have to rotate the fields and change the coordinates before the integration along the grating. Due to the polynomial dependence on the y', z' variables,

$$\boldsymbol{E}_Q(q_x, y', z', \omega) = e^{\left[iz'\left(\frac{\omega\cos(\varphi_I)}{\beta} + i\sin(\varphi_I)\mu\right)\right]}[\tilde{\boldsymbol{E}}_{Q_0}(q_x, y', \omega) + \tilde{\boldsymbol{E}}_{Q_1}(q_x, y', \omega)z' + \tilde{\boldsymbol{E}}_{Q_2}(q_x, y', \omega)z'^2]. \tag{A8}$$

The linear coordinate transformation (15) to y and z variables preserves this polynomial structure. Once again, the quadrupole contribution contains constant, linear, and quadratic terms in the z variable:

$$\boldsymbol{E}_Q(q_x, y, z, \omega) = e^{\left[iz\left(\frac{\omega\cos(\varphi_I)}{\beta} + i\sin(\varphi_I)\mu\right)\right]}[\boldsymbol{E}_{Q_0}(q_x, y, \omega) + \boldsymbol{E}_{Q_1}(q_x, y, \omega)z + \boldsymbol{E}_{Q_2}(q_x, y, \omega)z^2], \tag{A9}$$

where a z-dependent plane wave is multiplied by a second-order polynomial in the z variable, where the coefficients are some functions. The terms linear and quadratic in z contain the quadrupole contribution only and represent the nonparaxial contributions mentioned earlier.

3. Heisenberg equations for the quadrupole moments

Let us derive a general equation that describes the time dependence of the electric quadrupole momentum of a free scalar nonrelativistic packet $\psi(\boldsymbol{r}, t)$. Starting with the components of the current $j^\mu = \{j^0, \boldsymbol{j}\}$, which are

$$j^0(\boldsymbol{r}, t) = |\psi(\boldsymbol{r}, t)|^2, \quad \int d^3r\, j^0(\boldsymbol{r}, t) = 1, \quad \boldsymbol{j}(\boldsymbol{r}, t) = \psi^*(\boldsymbol{r}, t)\frac{-i}{2m}\nabla\psi(\boldsymbol{r}, t) + \text{c.c.}, \tag{A10}$$

we define the first three multipole moments corresponding to the initial state $\langle\psi|$, in the Heisenberg picture,

$$\boldsymbol{d}(t) = \langle\psi|\boldsymbol{r}(t)|\psi\rangle, \quad \boldsymbol{\mu}(t) = \frac{1}{2m}\langle\psi|\boldsymbol{r}(t) \times \boldsymbol{p}(t)|\psi\rangle,$$
$$Q_{\alpha\beta}(t) = \langle\psi|[3r_\alpha(t)r_\beta(t) - \boldsymbol{r}^2(t)\delta_{\alpha\beta}]|\psi\rangle, \tag{A11}$$

and the corresponding intrinsic values [11,30]

$$\boldsymbol{d}_{\rm int} = 0, \quad \boldsymbol{\mu}_{\rm int}(t) = \boldsymbol{\mu}(t) - \frac{1}{2m}\boldsymbol{d}(t) \times \langle\psi|\boldsymbol{p}(t)|\psi\rangle,$$
$$Q_{\alpha\beta,{\rm int}}(t) = Q_{\alpha\beta}(t) - 3d_\alpha(t)d_\beta(t) + \boldsymbol{d}^2(t)\delta_{\alpha\beta},$$
$$\alpha, \beta = 1, 2, 3. \tag{A12}$$

Only the intrinsic moments are considered throughout the paper, therefore the subscript "int" is omitted. The Hamiltonian of a free particle $H = \boldsymbol{p}^2/(2m)$ defines the equations of motion $i\partial_t A = [H, A]$ and well-known solutions

$$\boldsymbol{p}(t) = \boldsymbol{p}, \quad \boldsymbol{r}(t) = \boldsymbol{r} + \frac{\boldsymbol{p}}{m}t.$$

The Hamiltonian is quadratic in the momentum operator, and the quadrupole moment is quadratic in the position operator. From the Heisenberg equations, it follows that the third derivative of the quadrupole moment vanishes (it was obtained by direct calculations for the LG packet in Ref. [12]), thus, one can see that

$$Q_{\alpha\beta,{\rm int}}(t) = Q_{\alpha\beta,{\rm int}}(0) + Q^{(2)}_{\alpha\beta}t^2. \tag{A13}$$

[1] Y. Pan and A. Gover, Spontaneous and stimulated emissions of a preformed quantum free-electron wave function, Phys. Rev. A **99**, 052107 (2019).

[2] Z. Zhao, X.-Q. Sun, and S. Fan, Quantum Entanglement and Modulation Enhancement of Free-Electron–Bound-Electron Interaction, Phys. Rev. Lett. **126**, 233402 (2021).

[3] Y. Hu, Z. Li, B. Wetzel, R. Morandotti, Z. Chen, and J. Xu, Cherenkov radiation control via self-accelerating wave-packets, Sci. Rep. **7**, 8695 (2017).

[4] I. P. Ivanov and D. V. Karlovets, Detecting Transition Radiation from a Magnetic Moment, Phys. Rev. Lett. **110**, 264801 (2013).

[5] G. M. Lankhuijzen, M. Drabbels, F. Robicheaux, and L. D. Noordam, Decay of oriented Rydberg wave packets excited with far-infrared radiation, Phys. Rev. A **57**, 440 (1998).

[6] M. Stobińska, G. Alber, and G. Leuchs, Quantum electrodynamics of one-photon wave packets, Adv. Quantum Chem. **60**, 457 (2010).

[7] J. Peatross, C. Müller, K. Z. Hatsagortsyan, and C. H. Keitel, Photoemission of a Single-Electron Wave Packet in a Strong Laser Field, Phys. Rev. Lett. **100**, 153601 (2008).

[8] L. J. Wong, N. Rivera, C. Murdia, T. Christensen, J. D. Joannopoulos, M. Soljačić, and I. Kaminer, Control of quantum electrodynamical processes by shaping electron wavepackets, Nat. Commun. **12**, 1700 (2021).

[9] D. V. Karlovets and A. M. Pupasov-Maksimov, Nonlinear quantum effects in electromagnetic radiation of a vortex electron, Phys. Rev. A **103**, 012214 (2021).

[10] A. Pupasov-Maksimov and D. Karlovets, Smith–Purcell radiation of a vortex electron, New J. Phys. **23**, 043011 (2021).

[11] D. Karlovets, Dynamical enhancement of nonparaxial effects in the electromagnetic field of a vortex electron, Phys. Rev. A **99**, 043824 (2019).

[12] D. Karlovets and A. Zhevlakov, Intrinsic multipole moments of non-Gaussian wave packets, Phys. Rev. A **99**, 022103 (2019).

[13] V. B. Berestetskii, E. M. Lifshitz, and L. P. Pitaevskii, *Quantum Electrodynamics*, Vol. 4 (Butterworth-Heinemann, Oxford, UK, 1982).

[14] V. G. Bagrov, V. V. Belov, and A. Yu. Trifonov, Theory of spontaneous radiation by electrons in a trajectory-coherent approximation, J. Phys. A: Math. Gen. **26**, 6431 (1993).

[15] A. I. Akhiezer and N. F. Shulga, A theory of relativistic particle radiation in the quasi-classical approximation, Phys. Lett. A **144**, 415 (1990).

[16] A. I. Akhiezer and N. F. Shulga, Semiclassical theory of high-energy particle radiation in external fields, Phys. Rep. **234**, 297 (1993).

[17] V. N. Baier and V. M. Katkov, Processes involved in the motion of high energy particles in a magnetic field, Sov. Phys. JETP **26**, 854 (1968).

[18] R. Remez, A. Karnieli, S. Trajtenberg-Mills, N. Shapira, I. Kaminer, Y. Lereah, and A. Arie, Observing the Quantum Wave Nature of Free Electrons through Spontaneous Emission, Phys. Rev. Lett. **123**, 060401 (2019).

[19] D. V. Karlovets, G. Geloni, G. K. Sizykh, and V. G. Serbo, Generation of vortex particles via weak measurements. arXiv:2201.07997.

[20] I. Kaminer, M. Mutzafi, A. Levy, G. Harari, H. H. Sheinfux, S. Skirlo, J. Nemirovsky, J. D. Joannopoulos, M. Segev, and M. Soljačić, Quantum Čerenkov radiation: Spectral cutoffs and the role of spin and orbital angular momentum, Phys. Rev. X **6**, 011006 (2016).

[21] I. P. Ivanov, V. G. Serbo, and V. A. Zaytsev, Quantum calculation of the Vavilov-Cherenkov radiation by twisted electrons, Phys. Rev. A **93**, 053825 (2016).

[22] I. P. Ivanov and D. V. Karlovets, Polarization radiation of vortex electrons with large orbital angular momentum, Phys. Rev. A **88**, 043840 (2013).

[23] D. V. Karlovets and A. P. Potylitsyn, Generalized surface current method in the macroscopic theory of diffraction radiation, Phys. Lett. A **373**, 1988 (2009).

[24] J. H. Brownell, J. Walsh, and G. Doucas, Spontaneous Smith-Purcell radiation described through induced surface currents, Phys. Rev. E **57**, 1075 (1998).

[25] A. P. Potylitsyn, P. V. Karataev, and G. A. Naumenko, Resonant diffraction radiation from an ultrarelativistic particle moving close to a tilted grating, Phys. Rev. E **61**, 7039 (2000).

[26] H. L. Andrews, C. H. Boulware, C. A. Brau, and J. D. Jarvis, Dispersion and attenuation in a Smith-Purcell free electron laser, Phys. Rev. ST Accel. Beams **8**, 050703 (2005).

[27] B. J. McMorran, A. Agrawal, I. M. Anderson, A. A. Herzing, H. J. Lezec, J. J. McClelland, and J. Unguris, Electron vortex beams with high quanta of orbital angular momentum, Science **331**, 192 (2011).

[28] X. Zhong, J. Lin, S. Kao, Z. Liao, J. Zhu, X. Huang, R. Zhang, and H. L. Xin, Atomistic defect makes a phase plate for the generation and high-angular splitting of electron vortex beams, ACS Nano **13**, 3964 (2019).

[29] X. Zhong, S. Kao, J. Lin, Z. Liao, J. Zhu, X. Huang, R. Zhang, and H. L. Xin, High-angular splitting electron vortex beams generated by topological defects, Microsc. Microanal. **25**, 88 (2019).

[30] D. Karlovets, Relativistic vortex electrons: Paraxial versus nonparaxial regimes, Phys. Rev. A **98**, 012137 (2018).

[31] D. V. Karlovets, On the theory of polarization radiation in media with sharp boundaries, J. Exp. Theor. Phys. **113**, 27 (2011).

[32] See the code in the public repository [38].

[33] A. Renieri, Free electron generation of extreme ultraviolet coherent radiation: Theoretical aspects, in *Free Electron Generation of Extreme Ultraviolet Coherent Radiation*, AIP Conf. Proc. No. 118 (American Institute of Physics, Woodbury, NY, 1984), pp. 1–11.

[34] A. Friedman, A. Gover, G. Kurizki, S. Ruschin, and A. Yariv, Spontaneous and stimulated emission from quasifree electrons, Rev. Mod. Phys. **60**, 471 (1988).

[35] Calibration and Precision Angular Positioning (2021), https://www.rpiuk.com/calibration-and-precision-angular-positioning/.

[36] Note that Ref. [11] treats the fields at a distant point only, which simplifies the Lorentz transformations of angular variables. Here, we use the general formulas.

[37] M. Abramowitz and I. A. Stegun, *Handbook of Mathematical Functions with Formulas, Graphs, and Mathematical Tables*, Vol. 55 (U.S. Government Printing Office, Washington, DC, 1964).

[38] A. M. Pupasov-Maksimov, Smith-Purcell radiation by a vortex electron, https://github.com/pupasov/vortex-sp (2019).